Supporting Information

Constructing Z-scheme SnO_2/N-doped Carbon Quantum Dots/$ZnSn(OH)_6$ Nanohybrids with High Redox Ability for NO*x* Removal under VIS-NIR Light

Yanfeng Lu[a,b,d], Yu Huang[a,b,c,*], Jun-ji Cao[a,b,c], Haiwei Li[e], Wingkei Ho[f], Shun Cheng Lee[e]

[a] *Key Laboratory of Aerosol Chemistry and Physics, Institute of Earth Environment, Chinese Academy of Sciences, Xi'an 710061, China*

[b] *State Key Lab of Loess and Quaternary Geology (SKLLQG), Institute of Earth Environment, Chinese Academy of Sciences, Xi'an 710061, China*

[c] *CAS Center for Excellence in Quaternary Science and Global Change，Xi'an, 710061, China*

[d] *University of Chinese Academy of Sciences, Beijing 100049, China*

[e] *Department of Civil and Environmental Engineering, The Hong Kong Polytechnic University, Hung Hom, Hong Kong, China*

[f] *Department of Science and Environmental Studies, The Hong Kong Institute of Education, Hong Kong, China*

*Corresponding author: Prof. Yu Huang

E-mail address: huangyu@ieecas.cn

Tel: +86-02962336261

Fax: +86-02962336261

CONTENTS

Experimental section

Preparation of NCDs

NCDs was synthesized through a hydrothermal method. 3 g of citric acid and 3 g urea were mixed with 10 mL deionized water under vigorous stirring for 30 min. Then the solution was transferred to a 50 mL Teflon-lined stainless steel autoclave and heated at 180 °C for 4.5 h. After cooling down to room temperature, the dark green liquid was collected as NCDs by centrifugal treatment with 9000 rpm for 5 min.

Electrochemical analysis

The photocurrent response, electrochemical impedance spectra and flat band potential of the as-synthesized samples were detected by a Parstat4000 electrochemical workstation (USA) with a platinum plate and an Ag/AgCl electrode in a conventional three-electrode cell as the counter and reference electrodes, respectively. The photocurrent-time curves were measured at 0.2 V vs. Ag/AgCl in 0.5 mol·L^{-1} Na_2SO_3 at room temperature under irradiation with a 100 W LED lamp (λ = 420 nm). Electrochemical impedance spectroscopy (EIS) was conducted under open-circuit voltage in 1 mmol L^{-1} $K_3Fe(CN)_6$ and $K_4Fe(CN)_6$ solution. The flat band potential was measured through Mott−Schottky plots at a frequency of 1 kHz in 0.1 mol L^{-1} Na_2SO_4 (pH=7).

Photocatalytic performance measurements

The NO photo-oxidation activities of as-prepared sample were evaluated in a continuous-flow rectangular chamber with a volume capacity of 4.5 L (30 cm × 15 cm × 10 cm), which was similar to that in the ISO 22197-1 standard. Firstly, 0.2 g photocatalyst was spread on a glass dish (10.0 cm in diameter) and placed inside of the reactor. Then the gas stream with the 400 ppb NO, relative humidity of 30±5% and flow rate of 3 L/min, is prepared and fed to the chamber. A 300 W electric input Xenon lamp (Perfectlight, microsolar300, Beijing) is placed above the reactor. The light source with different wavelengths (simulated solar light, visible light, 365 nm, 450 nm, 550 nm, 700 nm, 800–1100 nm) was obtained by passing through the bandpass and cutoff filters. After the adsorption-desorption equilibrium the light source is turned on and the concentration of NO and NO_2 are quantified by a chemiluminescence NO*x* analyzer (Ecotech 9841, Australia). The efficiency of NO photo-oxidation at any given time was denoted as C/Co, where Co is the initial concentration and of NO, ppb.

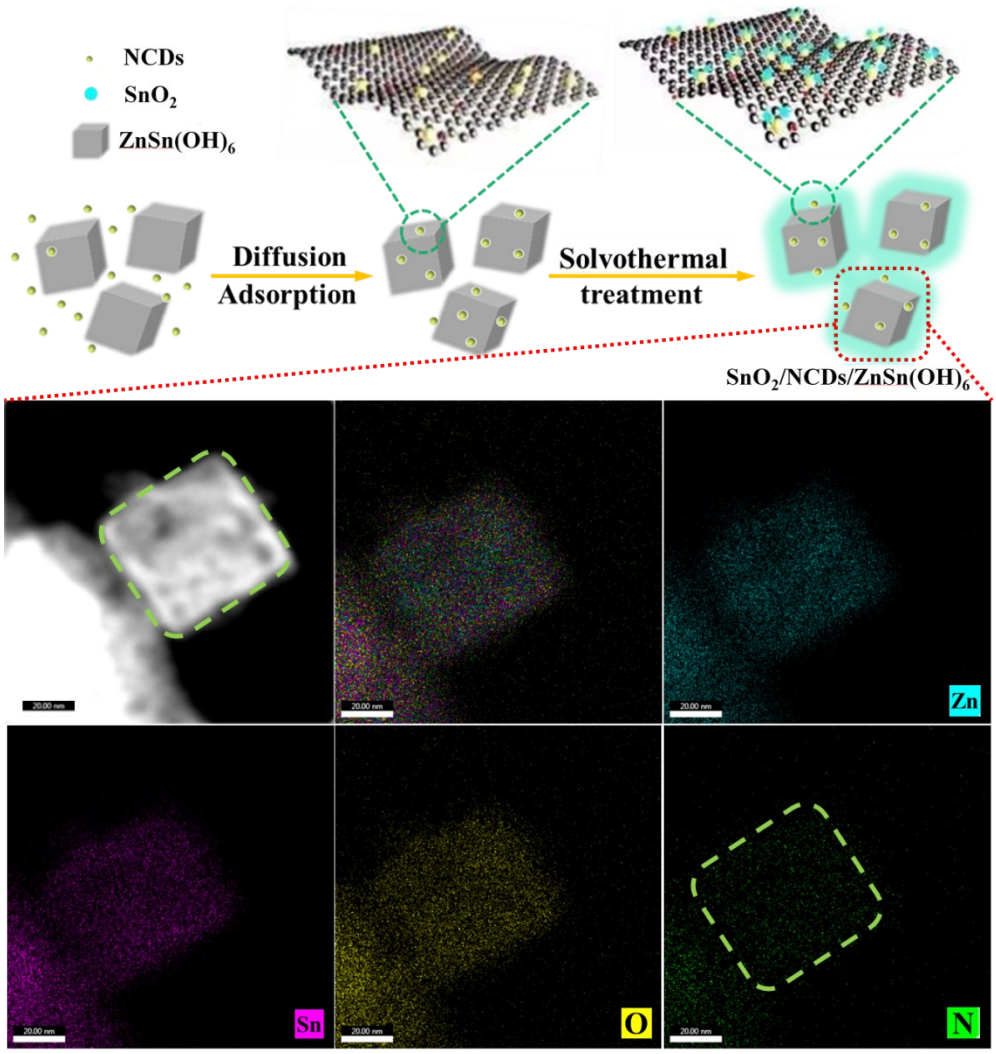

Scheme S1. Schematic diagram of *in-situ* synthesis process of SnO_2/NCDs/$ZnSn(OH)_6$ ternary Z-scheme nanohybrids.

A SnO_2/NCDs/ZHS Z-scheme photocatalyst is fabricated by an *in-situ* deposition of NCDs and SnO_2 cocatalyst on the surfaces of the nanoarchitecture mesoporous ZHS nanocubes. The typical synthesis of the SnO_2/ZHS nanocomposite decorated by NCDs is illustrated in Scheme 1. First, the ZHS nanocubes were generated in a continuously stirred reactor in ambient temperature. By adding the solution of NCDs into the precursor, the NCDs were tightly adsorbed on the surface of ZHS nanocubes due to hydrogen bond interactions. While

the solvothermal reaction was processed with pH~6.1, SnO_2 nanoparticles were obtained on the surface of ZHS, which due to the transform of $Sn(OH)_4$ during solvothermal reaction with pH~6.1: $Sn(OH)_4 \rightarrow SnO_2 + 2H_2O$.[1] During the solvothermal procedure, NCDs and SnO_2 nanoparticles was anchored homogeneously in situ on the nanoarchitecture mesoporous ZHS surface.

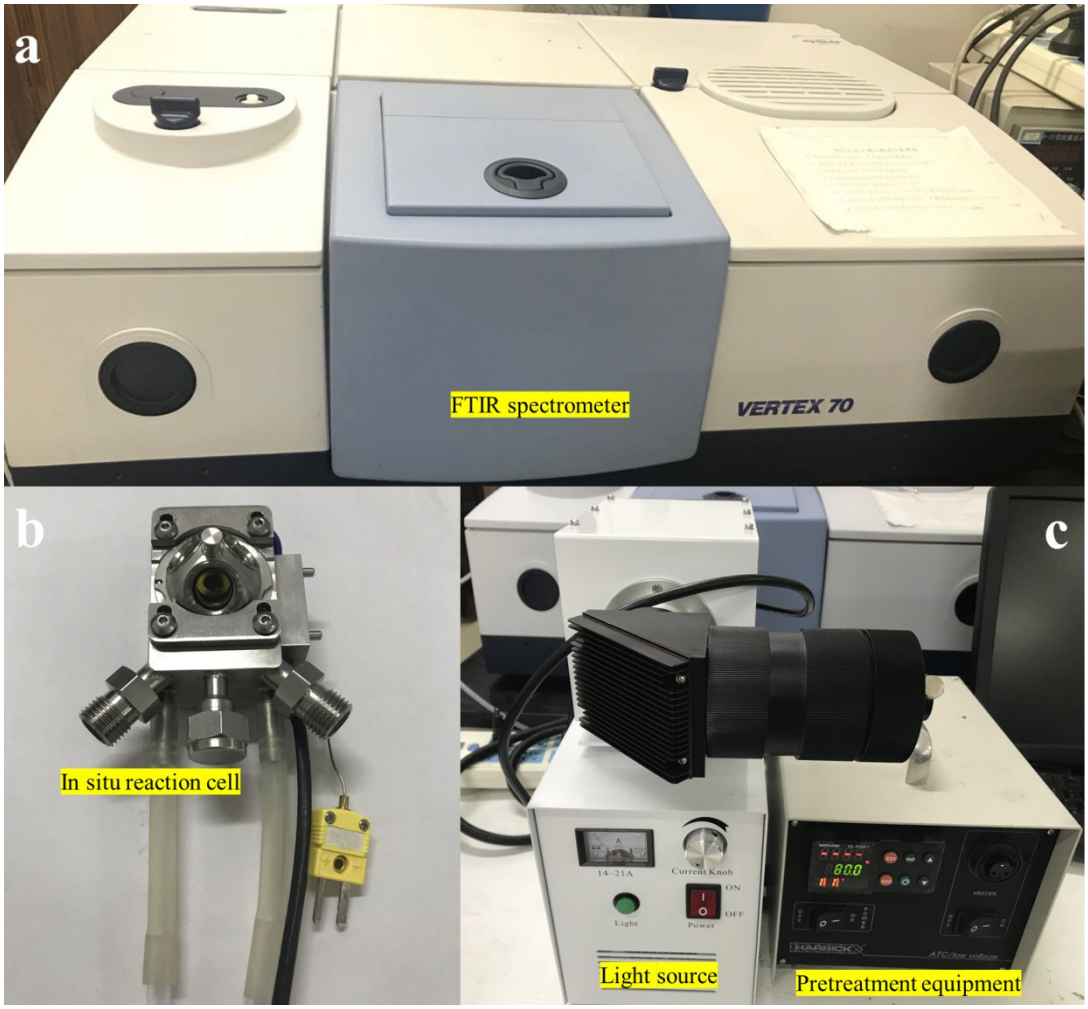

Scheme S2. (a) VERTEX 70 spectrometer (Bruker, Germany); (b) In situ reaction cell; (c) Pretreatment equipment and light source.

Table S1. Element atomic concentration of investigated catalysts by XPS measurement.

Catalyst	Atomic ratio (at. %)					Calculated	Calculated N	BET surface
	Zn 2p	Sn 3d	O 1s	C 1s	N 1s	SnO_2 ratio by XPS (at. %)	ratio by XPS (at. %)	area (m^2/g)
ZHS	11.8	10.9	59.6	17.7	/	/	/	172.7
SnO_2/NCDs/ZHS	10.8	12.1	54.6	22.1	0.4	12	3.7	105.6
NCDs	/	/	34.5	48.8	16.6	/	/	/

Table S2. Element analysis of as-prepared samples.

Catalyst	Weight (mg)	N%	C%	C/N	NCDs% (C)
ZHS	11.1	0.07	0.00	0.00	0
SnO_2/ZHS	15.7	0.05	0.06	1.2	0
NCDs/ZHS	58.2	1.27	4.14	3.25	4.14
SnO_2/NCDs/ZHS	55.8	1.18	3.04	2.58	3.04

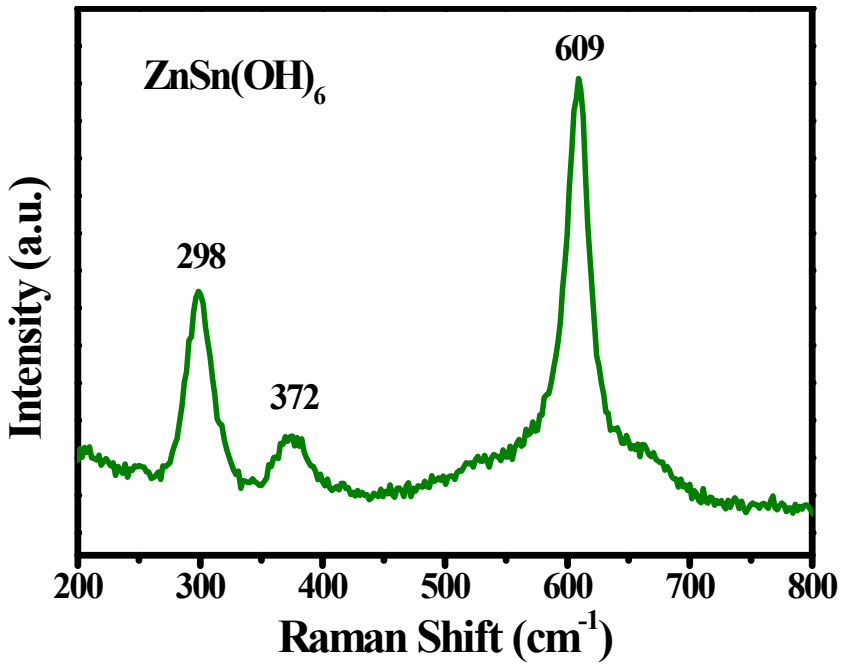

Fig. S1. Raman patterns of $ZnSn(OH)_6$.

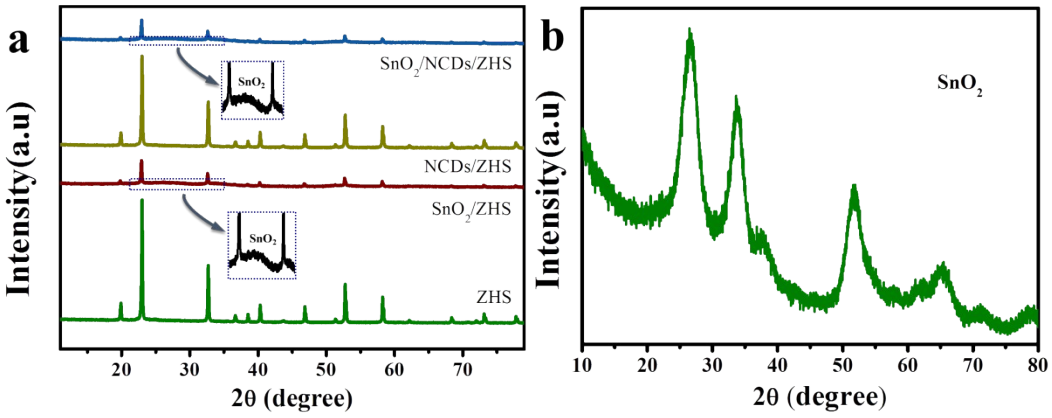

Fig. S2. XRD patterns of (a) all the as-prepared and (b) pure SnO_2 samples.

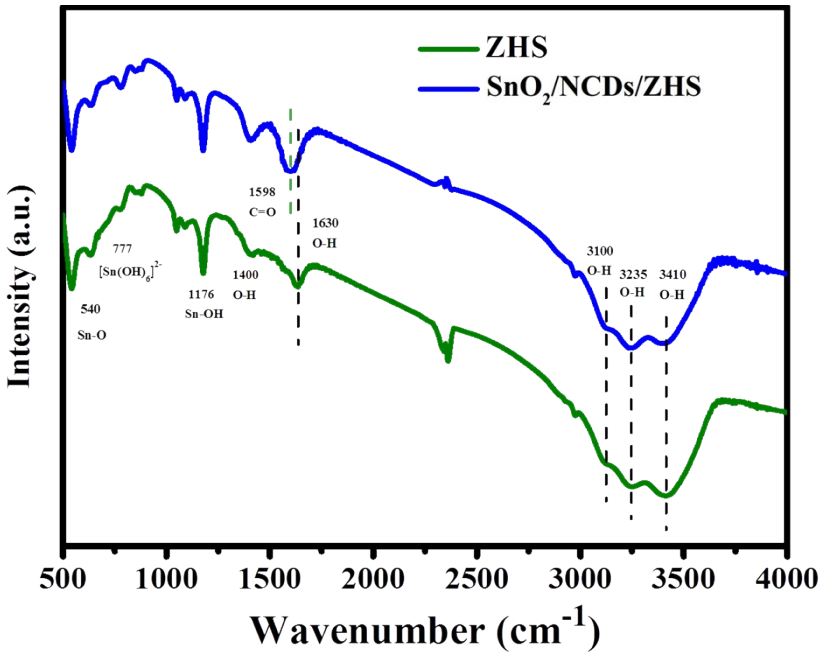

Fig. S3. FTIR spectra of ZHS and SnO_2/NCDs/ZHS.

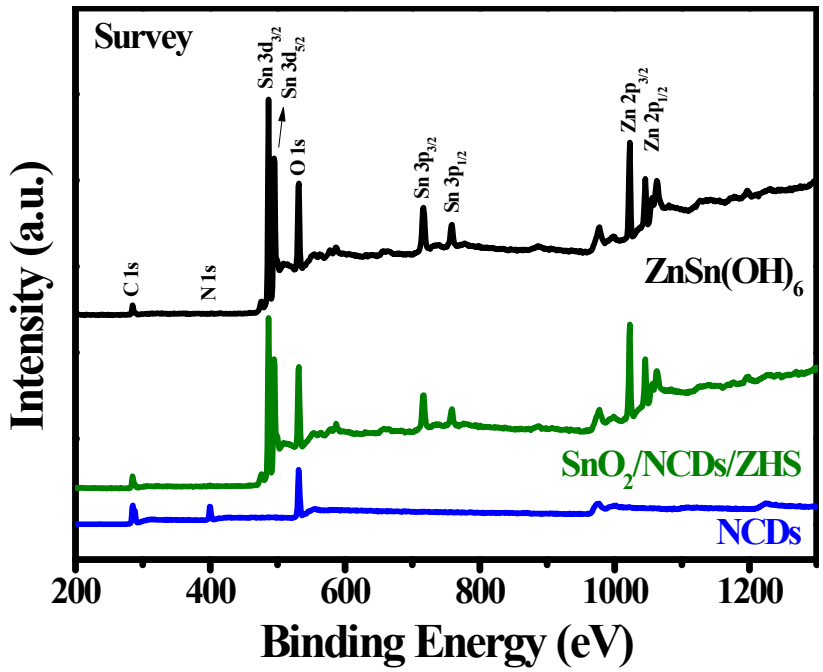

Fig. S4. XPS survey spectra of pure ZHS, NCDs and SnO_2/NCDs/ZHS nanohybrid.

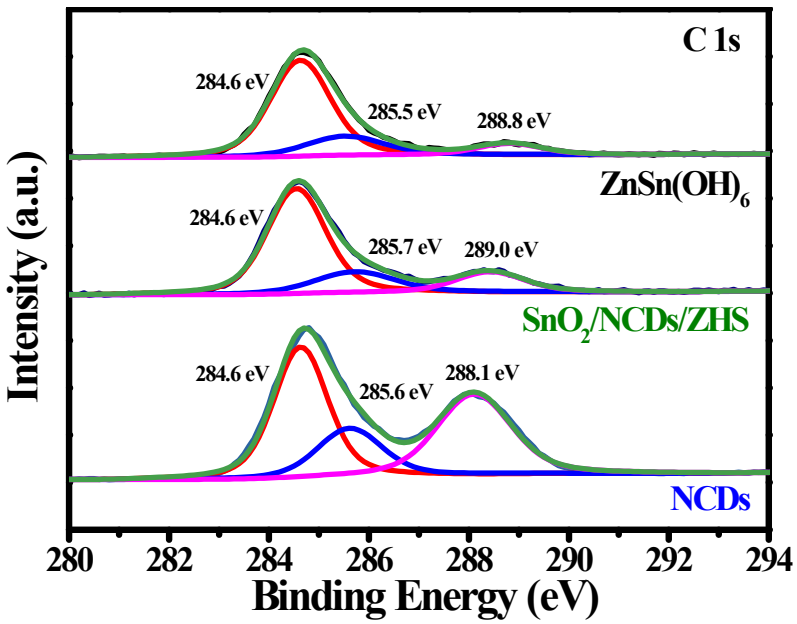

Fig. S5. The high-resolution XPS spectra of C 1s in pure $ZnSn(OH)_6$, NCDs and SnO_2/NCDs/ZHS nanohybrid.

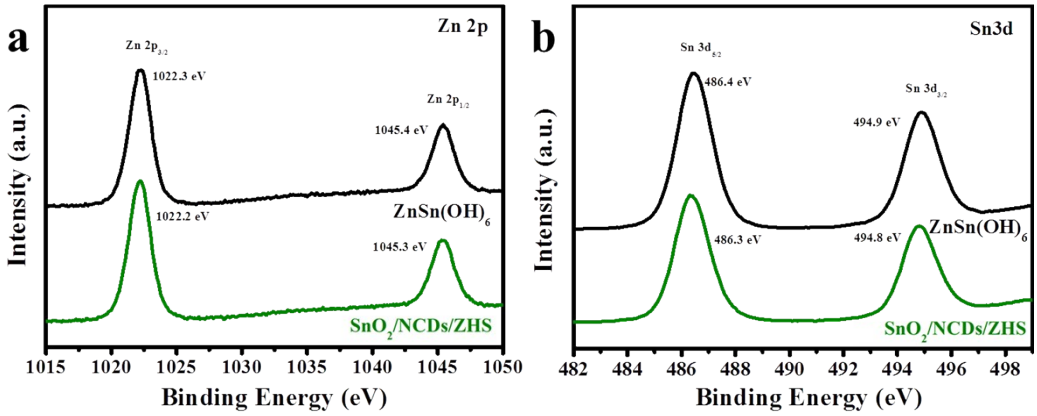

Fig. S6. The high-resolution XPS spectra of Zn 2p (a), Sn 3d (b) in pure $ZnSn(OH)_6$ and SnO_2/NCDs/ZHS nanohybrid.

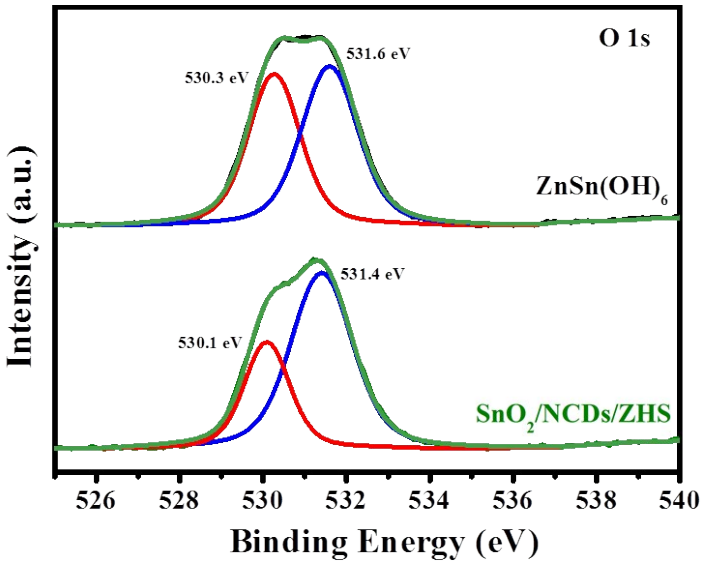

Fig. S7. The high-resolution XPS spectra of O 1s in pure $ZnSn(OH)_6$ and SnO_2/NCDs/ZHS nanohybrid.

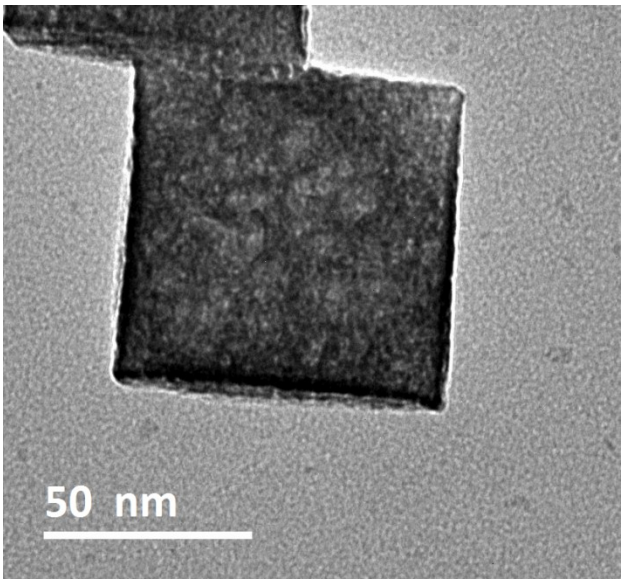

Fig. S8. TEM images of pristine ZHS nanocubes.

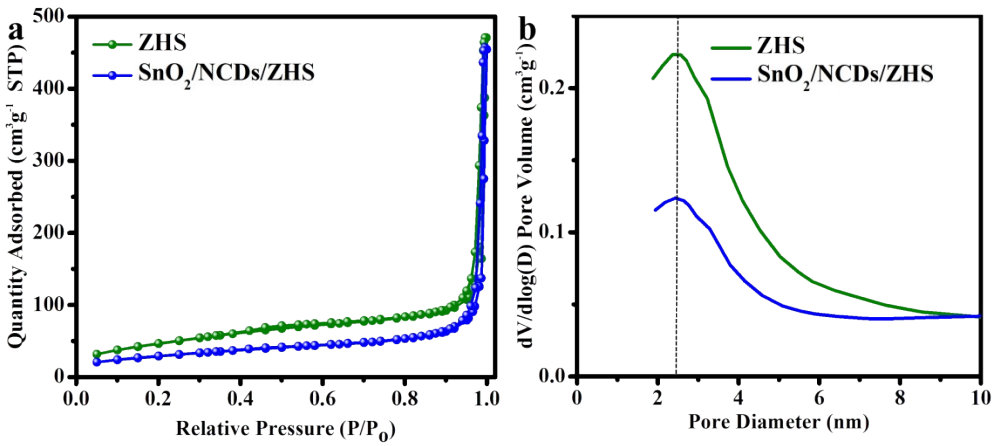

Fig. S9. (a) N_2 adsorption−desorption isotherms and (b) corresponding pore-size distribution curves of the pristine ZHS and SnO_2/NCDs/ZHS nanohybrid.

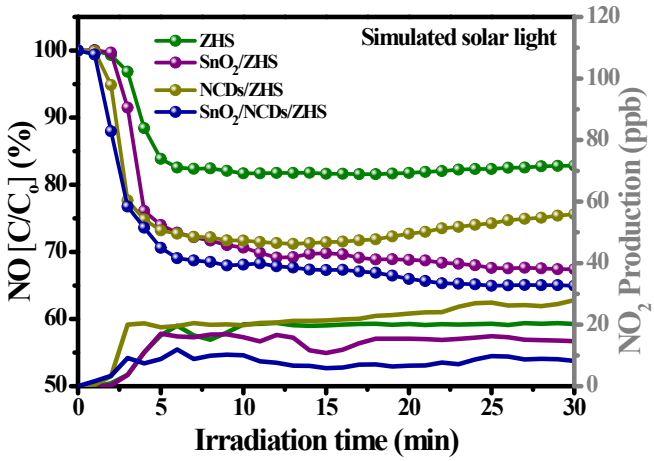

Fig. S10. Time profile of NO photocatalytic removal and the relative change NO_2 over different photocatalysts under simulated solar light irradiation.

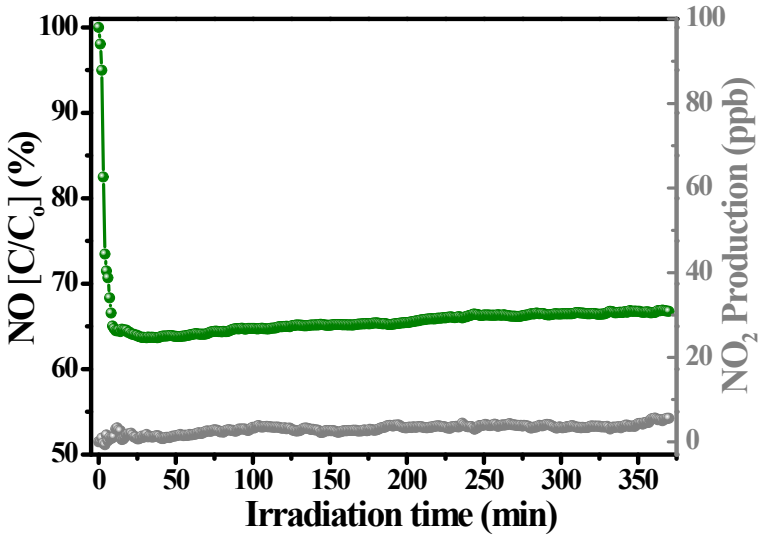

Fig. S11. Time profile of NO photocatalytic removal and the relative change NO_2 over SnO_2/NCDs/ZHS ternary nanohybrid for successive runs 375 min under visible-light irradiation.

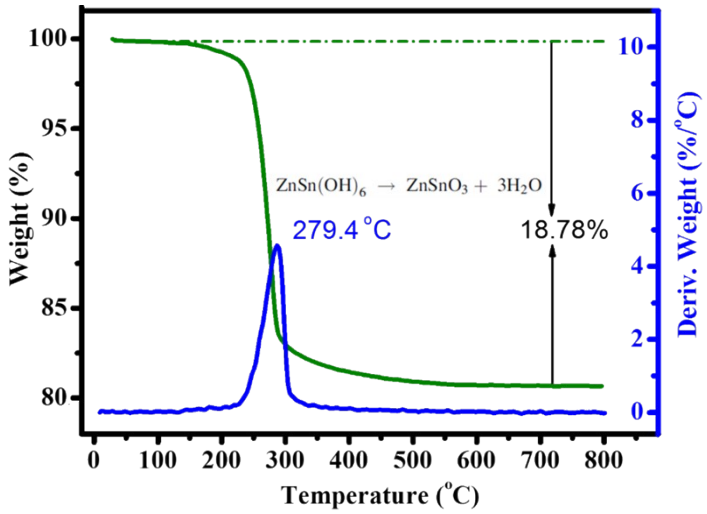

Fig. S12. TGA profiles of $ZnSn(OH)_6$ powders in air flow.

The thermal stability of the pristine ZHS precursor was also surveyed by thermogravimetric analysis (TGA), and the results showed that $ZnSn(OH)_6$ thermally decomposes at an elevated temperature (> 279 °C) with the decomposition reaction: $ZnSn(OH)_6 \rightarrow ZnSnO_3 + 3H_2O$,

Δm= − 18.8 % (Fig. S12).[2]

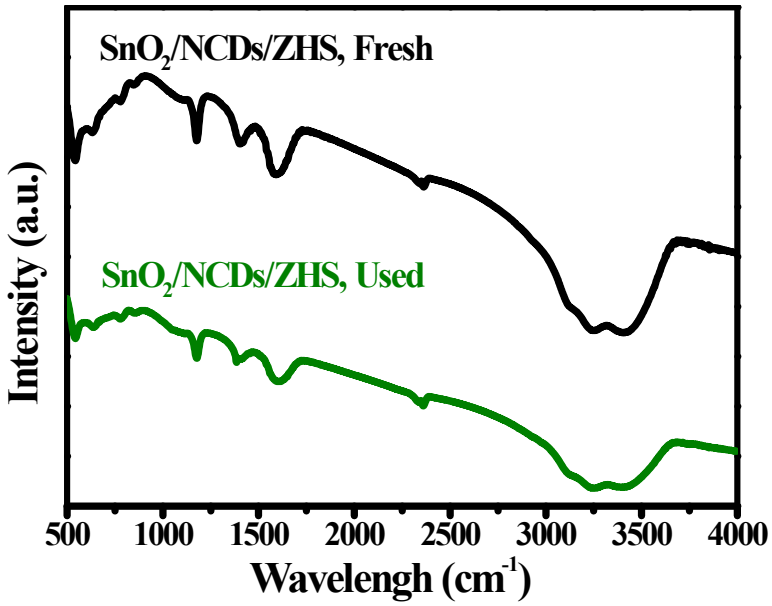

Fig. S13. FTIR spectra of SnO_2/NCDs/ZHS nanohybrid before and after the stability tests of successive runs 375 min.

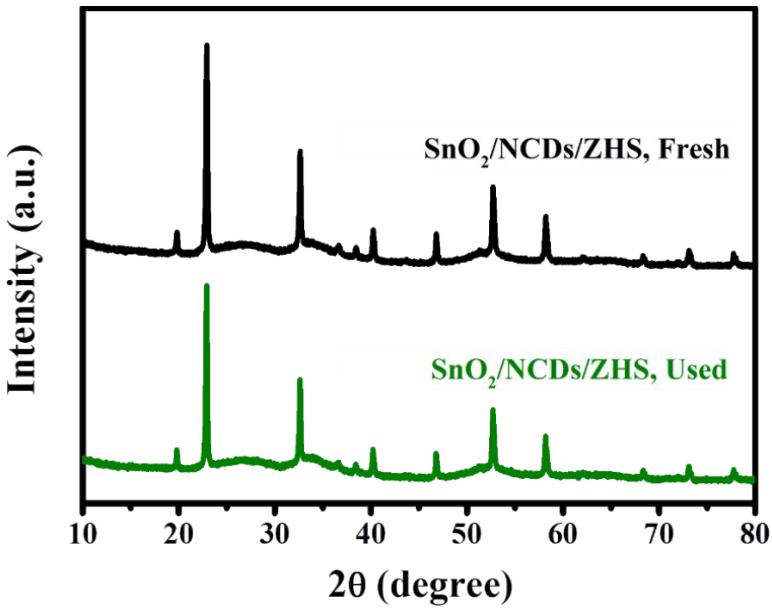

Fig. S14. XRD spectra of SnO_2/NCDs/ZHS nanohybrid before and after the stability tests of successive runs 375 min.

It can be observed that the optimized SnO_2/NCDs/ZHS ternary nanohybrid shows no apparent alterations in components (Fig. S13) or in the crystal structure (Fig. S14) under the same reaction conditions for successive runs 375 min tests in comparison with that before the photocatalytic reaction.

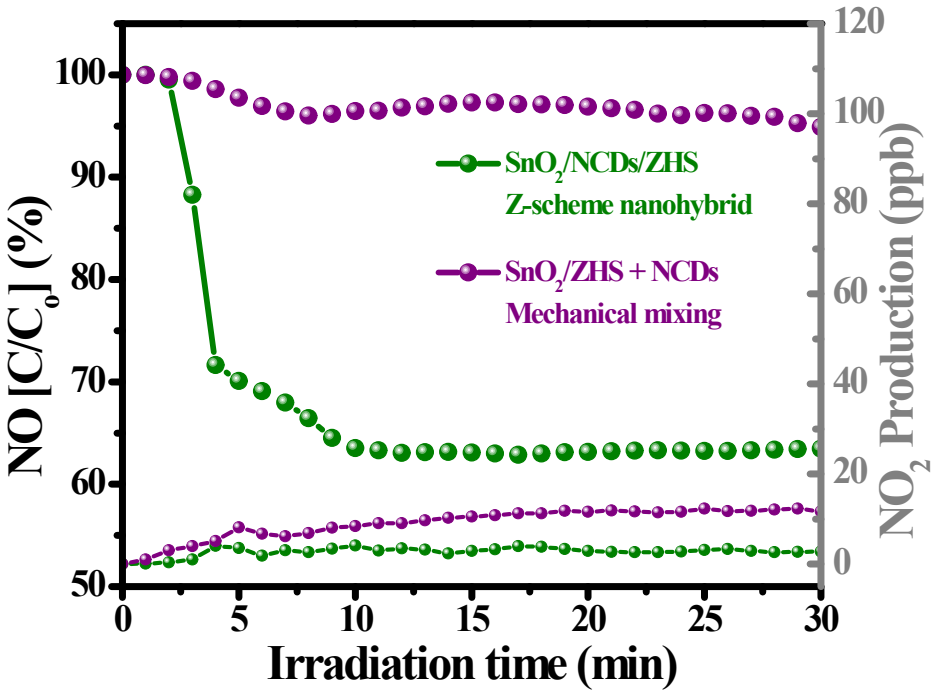

Fig. S15. The comparison of SnO_2/NCDs/ZHS ternary Z-scheme nanohybrid and mechanical mixing samples using SnO_2/ZHS and NCDs for NO photocatalytic removal and the relative change NO_2 under visible-light irradiation.

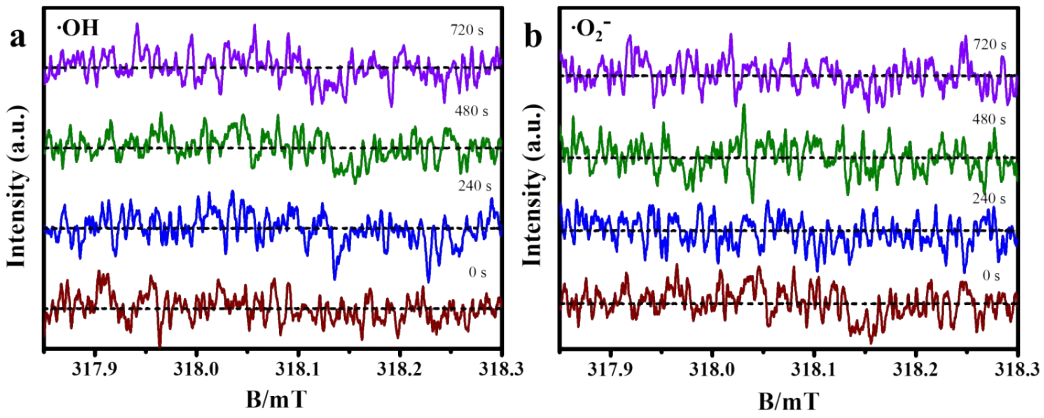

Fig. S16. Room temperature ESR spectra of pure ZHS during 12 min visible light irradiation, using DMPO as spin trapping agent.

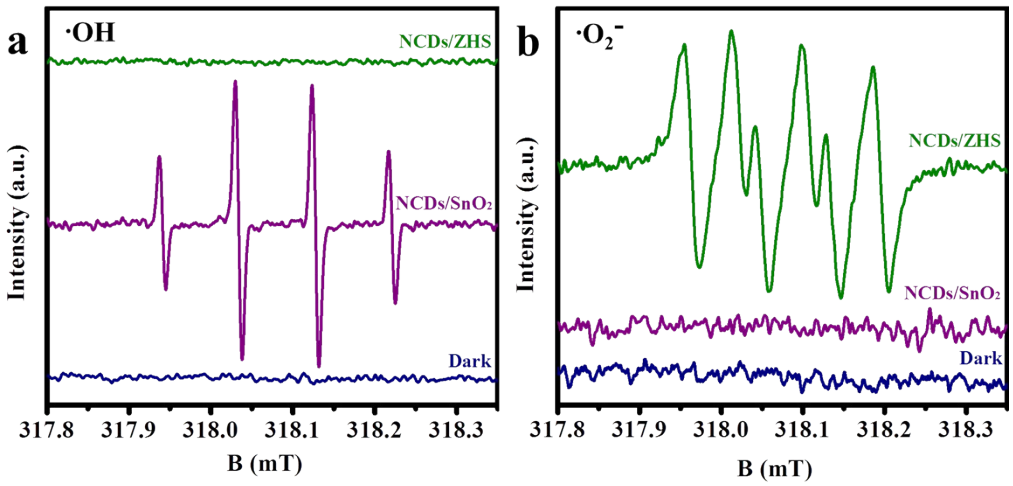

Fig. S17. Detection of (a) ·OH and (b) $\cdot O_2^-$ radicals over NCDs/SnO_2 and NCDs/ZHS under visible-light illumination ($\lambda \geq 420$ nm) by DMPO ESR spin trapping.

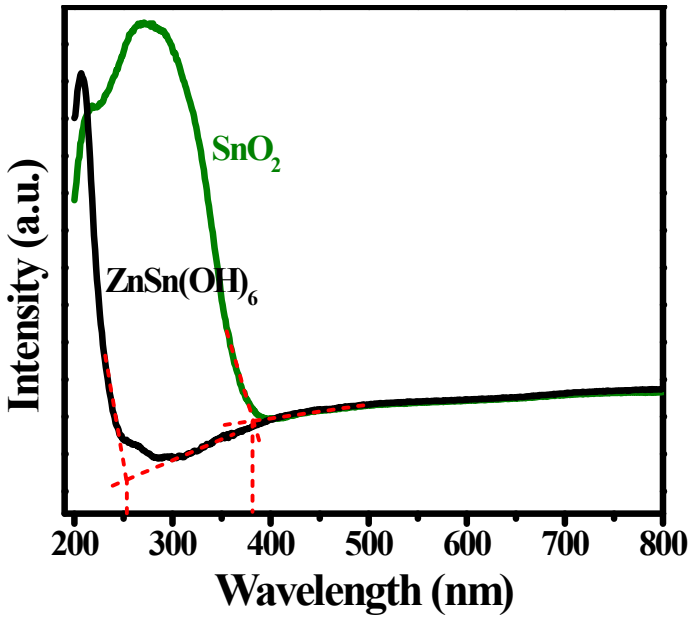

Fig. S18. UV–Vis absorption of pure $ZnSn(OH)_6$ and SnO_2 samples.

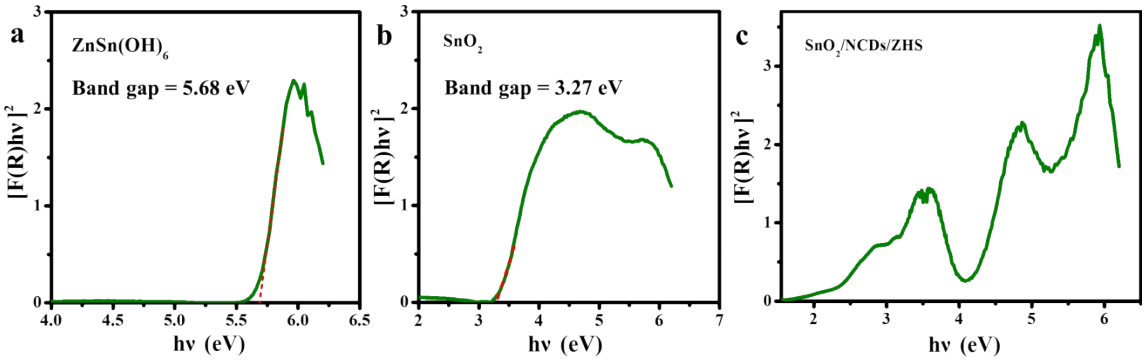

Fig. S19. Tauc plots of as-prepared ZHS, SnO_2 and NCDs/SnO_2/ZHS samples.

The band gap energies (Eg) of the prepared as-prepared pure ZHS and SnO_2 samples were determined using Tauc plot approach: $K(h\upsilon\text{-}Eg)^{1/n} = F(R)h\upsilon$, where K is a constant, $h\upsilon$ is photon energy, F(R) is the absorption coefficient and n equals 2 for direct transition of ZHS and SnO_2.

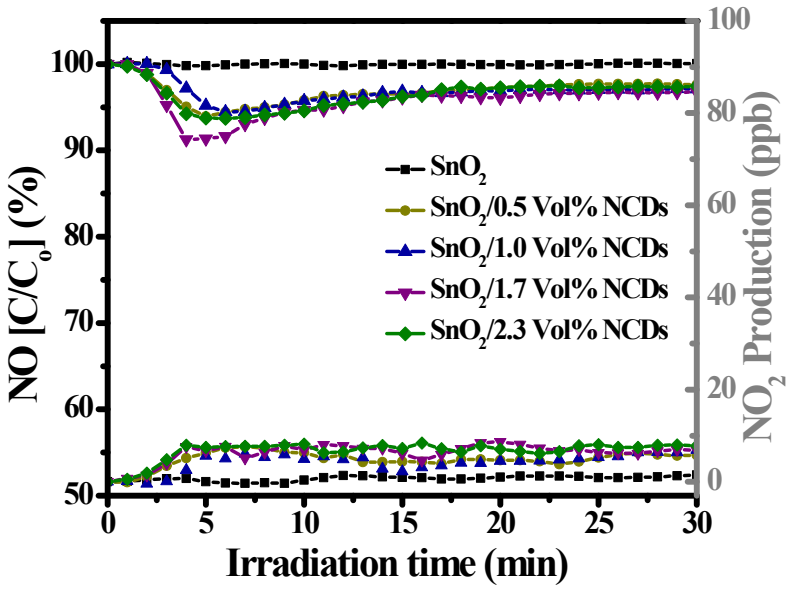

Fig. S20. Time profile of NO photocatalytic removal and the relative change of NO_2 over pristine SnO_2 and SnO_2/NCDs nanocomposite with different volume ratio of NCDs solution under visible-light irradiation.

The controllable contrast samples of SnO_2/NCDs nanocomposites with different volume ratio of NCDs were prepared by similar solvothermal method. 0.7 g of $SnCl_4 \cdot 5H_2O$ and 0.4 g NaOH was first dissolved in 15mL deionized water and 20 mL ethanol. The mixture was kept stirring for 7 h and maintained pH to 6.1 using sodium hydroxide solution (2 M). The mixture was transferred to a 50 mL Teflon-lined stainless steel autoclave and maintained at 160 °C for 12 h. The resulting composites were washed with ethanol and water three times, and dried at 60 °C for 12 h to obtain the pure SnO_2. The SnO_2/NCDs nanocomposites with different volume ratio of NCDs were prepared by change the volume ratio of NCDs solution. We changed the volume of addition of NCDs solution with different volume ratios (0.5/1.0/1.7/2.3 %), keeping all other conditions unchanged.

The controllable contrast samples of SnO_2/NCDs nanocomposites with the different

volume ratio of NCDs were prepared to removal NO under visible-light irradiation. Fig. S20 shows the photocatalytic activities over the SnO_2/NCDs nanocomposites with different volume ratio of NCDs are almost no change and remain around 5%, which illustrated there is no evident impact for the NO removal rate with the amount change of NCDs. This indicates that the amount change of NCDs in SnO_2/NCDs system is incapable of assisting in the generation of more reactive oxygen species during the photocatalytic reaction.

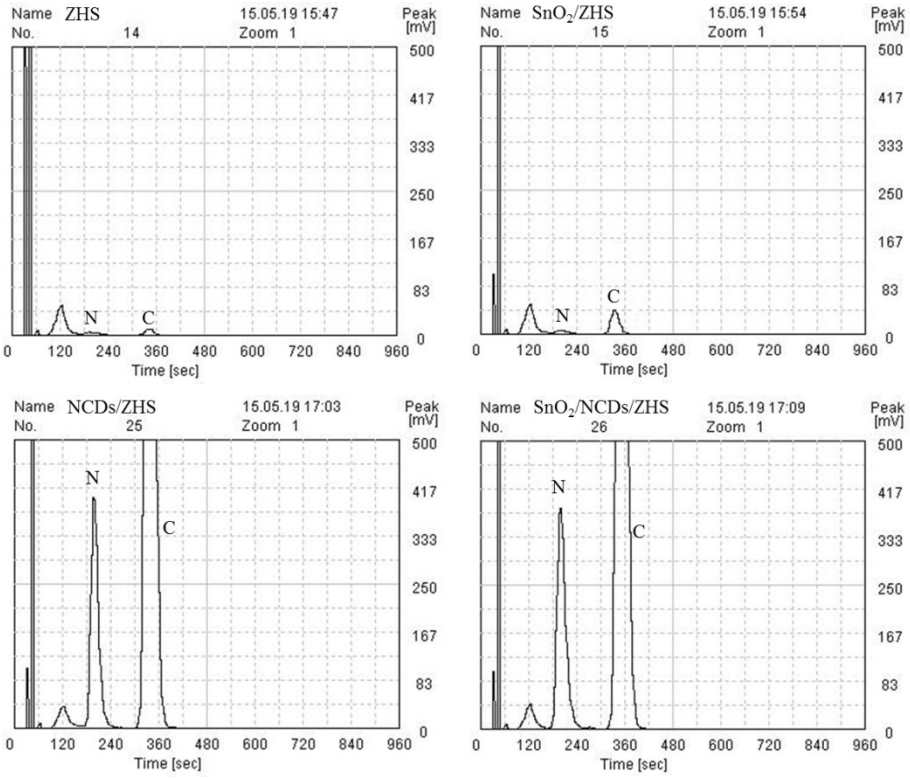

Fig. S21. The time scale element profiles.

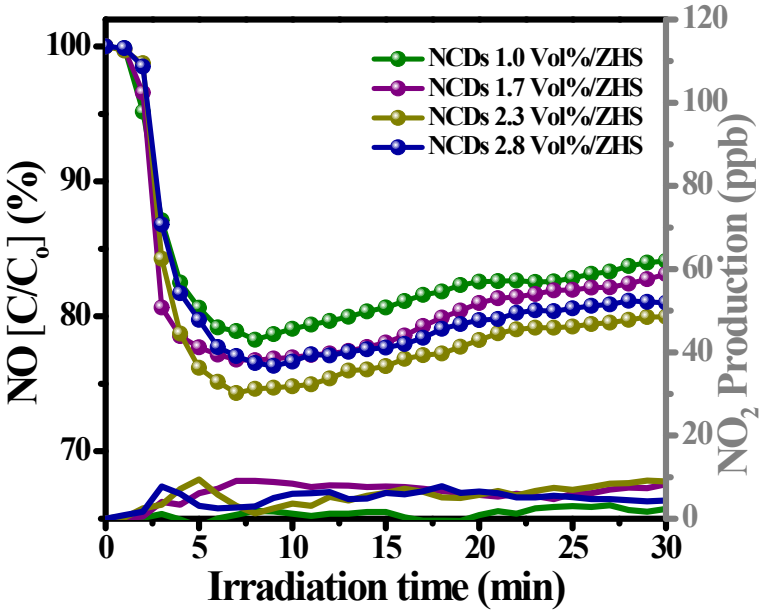

Fig. S22. Time profile of NO photocatalytic removal and the relative change of NO_2 over NCDs/ZHS nanocomposites with different volume ratio of NCDs under visible light ($\lambda \geq 420$ nm) irradiation.

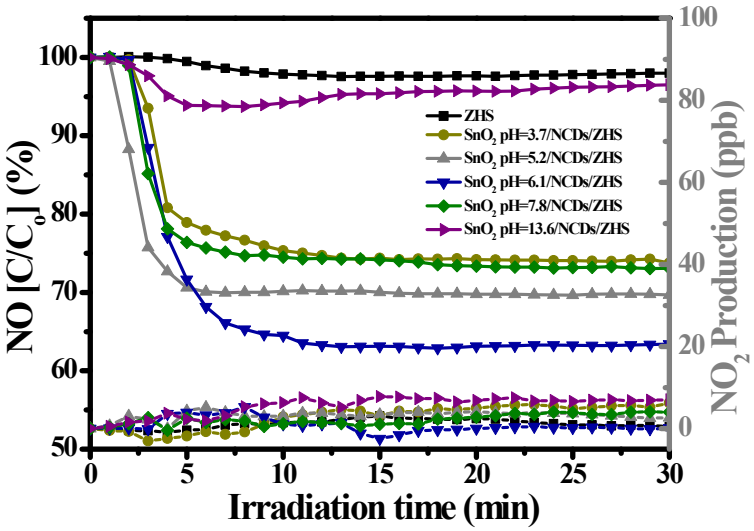

Fig. S23. Time profiles of NO photocatalytic removal and the relative change of NO_2 over pristine ZHS and SnO_2/NCDs/ZHS Z-scheme nanohybrids with different loading amount of SnO_2 under visible-light irradiation.

The SnO_2/NCDs/ZHS ternary nanohybrids with different quality of SnO_2 sample were prepared by change the pH of precursor solution. We adjusted and maintained the pH of the mixture to 3.7, 5.2, 6.1, 7.8 and 13.6 using sodium hydroxide solution (2M/5M), keeping all other conditions unchanged.

To further understand the role of SnO_2 in SnO_2/NCDs/ZHS ternary Z-scheme nanohybrids, the NO removal rate over ternary Z-scheme photocatalysts with different quality of SnO_2 (the loading quality of SnO_2 decreased with increasing of solution pH) were displayed under visible-light irradiation.[3] Fig. S23 shows the photocatalytic NO removal rate increases initially with decreasing of the loading quality of SnO_2 and then reaches a maximum when the amount of SnO_2 is about 12% (pH ~ 6.1, Calculated SnO_2 ratio by XPS). It can be seen that NO removal rate over SnO_2/NCDs/ZHS ternary Z-scheme nanohybrids with pH ~ 13.6 (SnO_2 ratio is trending to 0%) was evaluated to be 5% under visible-light irradiation for 30 min, which is much lower than that of SnO_2/NCDs/ZHS ternary Z-scheme nanohybrids with 12% SnO_2 (37%). This behavior can be attributed to the fact that a further increase in the amount of SnO_2 leads to a decrease in the NO removal rate, due to the completely encased surface on ZHS impeding the contact of ZHS and NCDs by the excessive loading of SnO_2, which blocked the photo-induced electrons transfer from NCDs to the CB of ZHS. Therefore, an appropriate SnO_2 loading amount is a key factor in achieving optimized photocatalytic activity of SnO_2/NCDs/ZHS ternary Z-scheme nanohybrids.

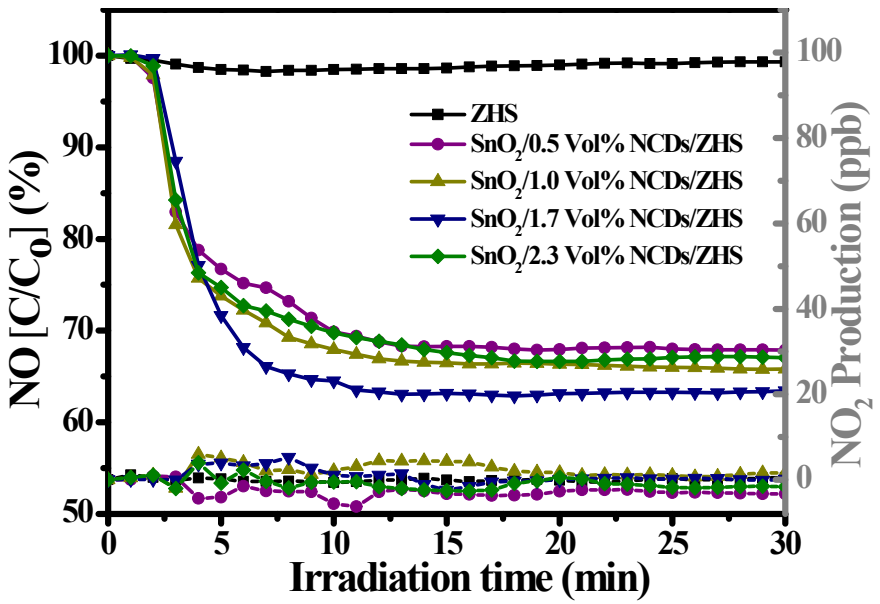

Fig. S24. Time profile of NO photocatalytic removal and the relative change of NO_2 over pristine ZHS and SnO_2/NCDs/ZHS Z-scheme nanohybrids with different volume ratio of NCDs solution under visible-light irradiation.

All controllable contrast samples were prepared by similar solvothermal method. The SnO_2/NCDs/ZHS ternary Z-scheme nanohybrids with different volume ratio of NCDs were prepared by change the volume ratio of NCDs solution. 0.7 g of $SnCl_4 \cdot 5H_2O$ and 0.4 g NaOH was first dissolved in 15 mL deionized water and was stirred for 30 min. 0.4 g of $(CH_3COO)_2Zn \cdot 2H_2O$ was dispersed in 20 mL ethanol with ultrasounds for 30 min and then was added into the previous solution dropwise. The mixture was kept stirring for 7 h and maintained pH to 6.1 using sodium hydroxide solution (2M).Subsequently, the NCDs solution with different volume ratios (0.5/1.0/1.7/2.3 %) was added into the above solution with stirring for 1 h and transferred to a 50 mL Teflon-lined stainless steel autoclave and maintained at 160 °C for 12 h. The resulting composites were washed with ethanol and water three times, and dried at 60 °C for 12 h to obtain the SnO_2/NCDs/ZHS ternary nanohybrids

with different volume ratio of NCDs.

To investigate how the NCDs influence the photocatalytic activity of the Z-scheme nanohybrids, we further evaluated the visible-light photocatalytic removal NO activities ($\lambda \geq$ 420 nm) of the resultant SnO_2/NCDs/ZHS Z-scheme nanohybrids with different amounts of NCDs. As presented in Fig. S24, compared with pristine ZHS, the efficiency of NO removal over the SnO_2/NCDs/ZHS nanohybrids with different amounts of NCDs are significantly enhanced, while the production of NO_2 is trending to 0 ppb. An appropriate NCDs loading amount (Vol 1.7%) is capable of assisting in the absorption of visible light and the transfer of photo-induced electron at the semiconductor interface, which is a key factor in achieving optimized photocatalytic activity of SnO_2/NCDs/ZHS ternary Z-scheme nanohybrids.

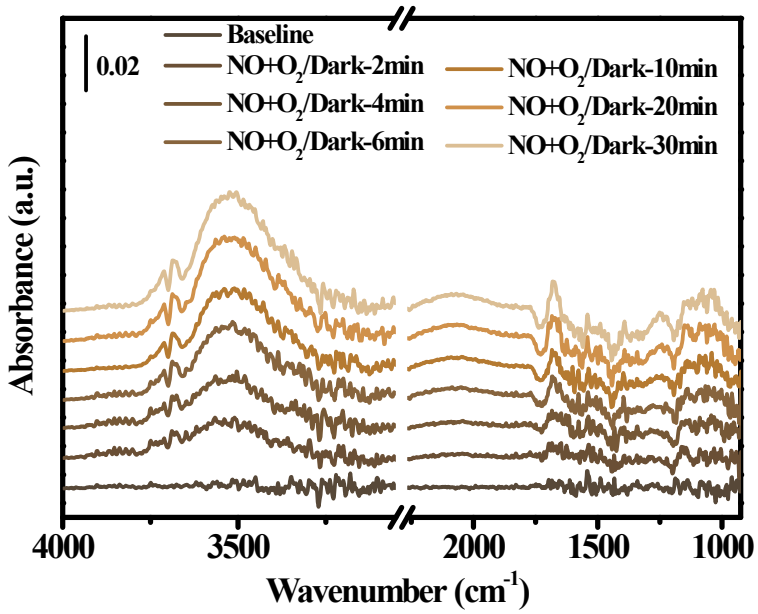

Fig. S25. In situ IR spectra of SnO_2/NCDs/ZHS Z-scheme photocatalyst during adsorption process in the dark.

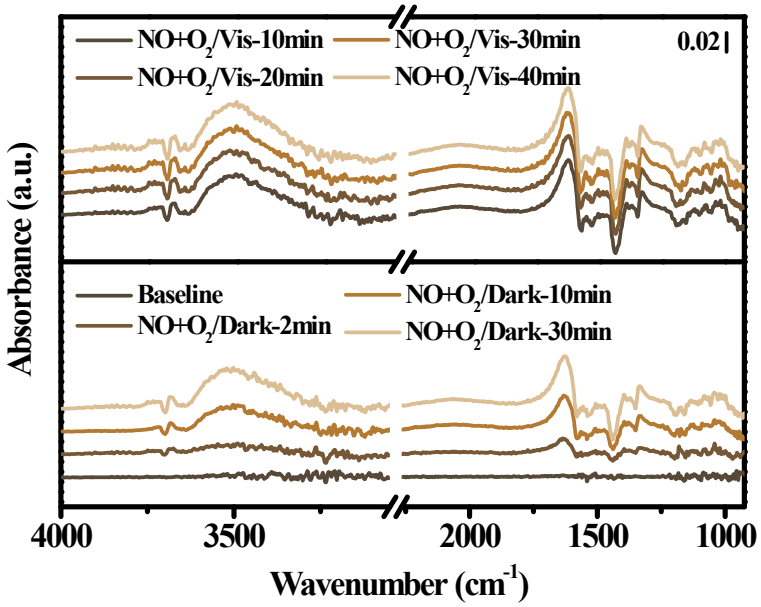

Fig. S26. In situ IR spectra of pristine ZHS during adsorption process in the dark and photocatalytic NO oxidation under visible light irradiation.

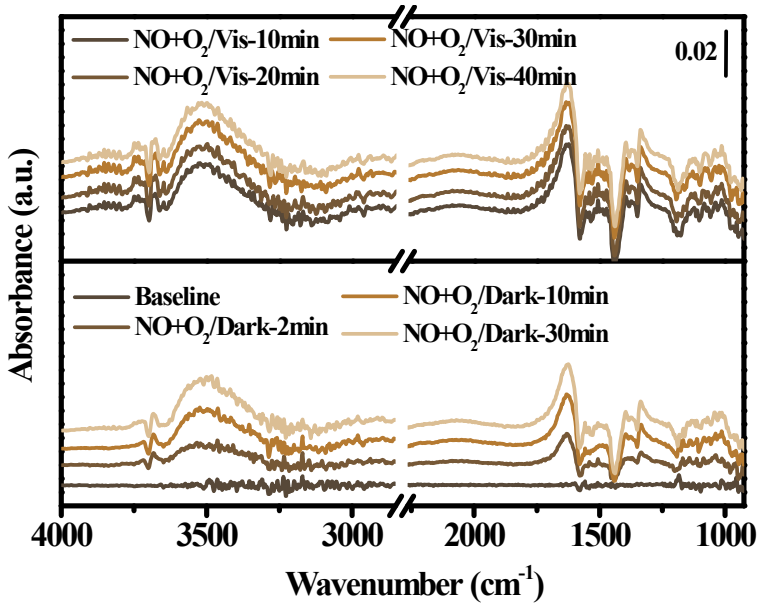

Fig. S27. In situ IR spectra of SnO_2/ZHS nanocomposite during adsorption process in the dark and photocatalytic NO oxidation under visible light irradiation.

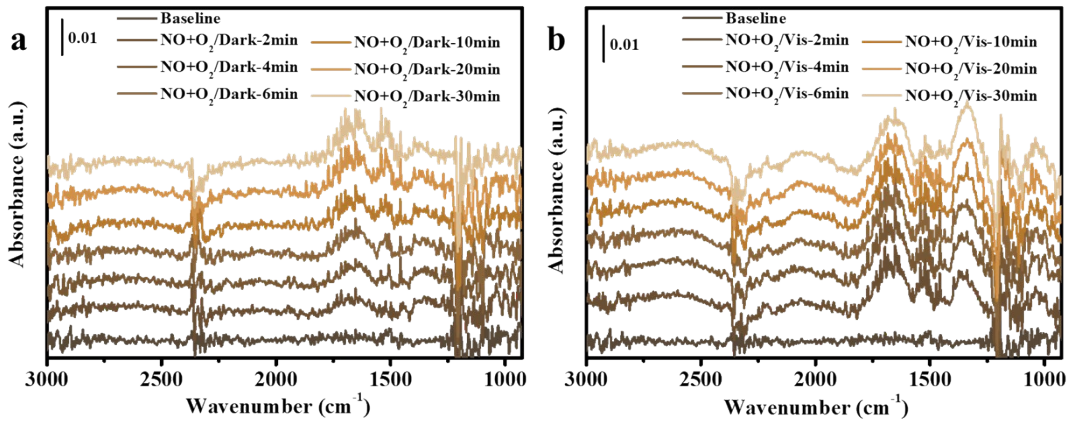

Fig. S28. In situ IR spectra of NCDs/ZHS nanocomposite (a) during adsorption process in the dark and (b) photocatalytic NO oxidation under visible light irradiation.

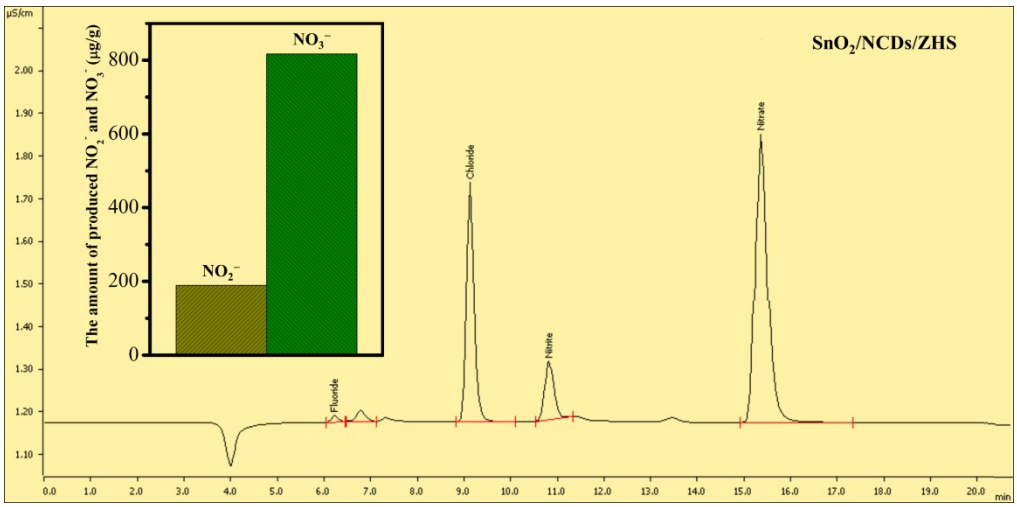

Fig. S29. The time scale IC profiles. The inset is the production amount of NO_2^- and NO_3^- over SnO_2/NCDs/ZHS sample.

References

1 C. Chen, X. Zheng, J. Yang and M. Wei, Phys. *Chem. Chem. Phys.*, 2014, **16**, 20073-20078.

2 X. Fu, D. Huang, Y. Qin, L. Li, X. Jiang and S. Chen, *Appl. Catal. B*, 2014, **148-149**, 532-542.

3 X. Fu, J. Wang, D. Huang, S. Meng, Z. Zhang, L. Li, T. Miao and S. Chen, *ACS Catal.*, 2016, **6**, 957-968.